

Improving robustness to noise of nonlinear parameter identification using control-based continuation

Sandor Beregi, David A. W. Barton, Djamel Rezgui, Simon A. Neild

Faculty of Engineering, University of Bristol, Bristol, United Kingdom

Abstract

In this study, we consider the experimentally-obtained, periodically-forced response of a nonlinear structure in the presence of noise. Control-based continuation is used to measure both the stable and unstable periodic solutions while different levels of noise are injected into the system. Using this data, the robustness of the control-based continuation algorithm and its ability to capture the noise-free system response is assessed by identifying the parameters of an associated Duffing-like model. We demonstrate that control-based continuation extracts system information more robustly, in the presence of a high level of noise, than open-loop parameter sweeps and so is a valuable tool for investigating nonlinear structures.

1. Introduction

Studying physical structures experimentally can be a challenge if the measurements are polluted with a significant amount of noise. Often information is lost and it becomes difficult to resolve the fine details of the experiment's behaviour. In this paper, we propose control-based continuation as an approach for robust parameter identification in noisy nonlinear systems. By tracking the steady-state solutions, we analyse a noise-contaminated experimental rig featuring nonlinear characteristics and assess the performance of the control-based continuation algorithm benchmarked against open-loop parameter sweeps.

Investigating nonlinear systems is a long-established field of dynamical analyses [11]. Nonlinear dynamical models have been used effectively to explain phenomena in many engineering applications [16] as well as in many other areas such as, amongst others, biological [12] or economical [6] systems.

From a practical point a view, an essential part of analysing nonlinear phenomena is building models which represent the relevant features of the system. This is often achieved using reduced-order mathematical models, which requires the identification of the model parameters.

In the literature, there are numerous studies advocating a range of different methods for parameter identification. In engineering applications, a common solution is to measure the electrical or mechanical restoring force of the system and directly identify the system parameters as shown by Masri et al [20] and Cammarano et al [8]. While this approach can be effective in characterising the system, the required measurements can be difficult to carry out in some cases. Therefore, many papers focus on methods that identify model parameters based on the observed dynamical behaviour. Kerschen et al [14] and Noel and Kerschen [24] give a thorough review covering a range of different techniques of nonlinear system identification. A number of these methods, such as nonlinear auto-regressive moving average with exogenous inputs (NARMAX) modelling [17, 18] or the use of the Hilbert transform are based on the analysis of time series [9]. Goharoodi [10] and Marchesiello [19] perform nonlinear subspace identification by a time-domain study of the system response for a given excitation. A similar approach is followed by Narayanan [21] using multi-harmonic excitation. Noel and Kerschen carry out a similar identification of nonlinear subspaces in the frequency domain [23] reducing the computational burden of the method [26].

Another possible strategy is to extend the theory of (linear) modal analysis to nonlinear systems by considering nonlinear normal modes [30, 33] and measuring the nonlinear frequency response diagram of the structure [25].

In practice, the frequency-response of a system can be obtained in several ways for example by applying random excitation or impulses to the system. In our study, we focus on the commonly-used approach where the frequency-response is extracted by performing parameter-sweeps. However, nonlinear systems may have specific (so-called bistable) parameter domains where two (or even more) stable steady-state solutions exist for the same set of parameters. The boundary of the domains of attraction of these stable solutions is referred to as a separatrix which can be often characterised by another, unstable, steady-state solution. In an experiment, one can observe this as a sensitivity of the steady-state behaviour to the initial conditions. For example, one may find that a certain level of perturbation is tolerable and so the dynamics stay within the same basin of attraction, while a larger perturbation may lead the system to diverge from its originally observed steady-state

behaviour. This phenomenon also means that by standard parameter-sweeps, only stable solutions can be captured. Thus, part of the bifurcation diagram may remain hidden. The presence of noise can also contribute to the loss of data by potentially driving the system away from a stable solution with a small domain of attraction.

Continuation methods trace a family of solutions in a nonlinear system by applying small parameter changes to follow the solution branch. In case of mathematical models, several analytical or numerical techniques, based on bifurcation analysis, are available to track steady-state solutions irrespective of their stability [15]. Numerical continuation methods, in particular, are constructed around solving a nonlinear zero problem. For example, periodic solutions are commonly calculated using the method of collocation to discretise the solution over the time-period while the solution branch is continued with the pseudo-arc length method with respect to a system parameter, referred to as bifurcation parameter [29].

Control-based continuation [31] is a method which incorporates the techniques of numerical continuation and bifurcation analysis to trace solutions of physical and numerical experiments where the governing equations are not explicitly available. Thus, in principle, it is capable of capturing both stable and unstable steady-state solutions. Just as is the case for numerical bifurcation analysis, periodic solutions have to be discretised and composed into an equivalent zero problem, e.g. by the coefficients of their truncated Fourier series. These coefficients can be used to design a control which is stabilising and non invasive; that is, the steady-state solutions of the controlled system are the same as the steady-state response of the open-loop system.

In our study, we apply the method of control-based continuation to conduct the experimental bifurcation analysis of a forced nonlinear oscillator subjected to noise. The acquired data is then used to identify parameters for a model of the structure based on the assumption it is a one-degree-of-freedom Duffing-like oscillator, which we use as a model of the experimental rig. Physically polluting the system with different levels of noise, we assess the robustness of control-based continuation derived data to random perturbations. This is an important factor from the point of view of the practical effectiveness of the method as, in general, a heavy noise-load may result in losing relevant information from the system. The robustness of control-based continuation is tested and compared against parameter sweeps without control. Thus, we assess if control-based continuation is capable to capture the response more accurately and if it is capable to reveal details from the system

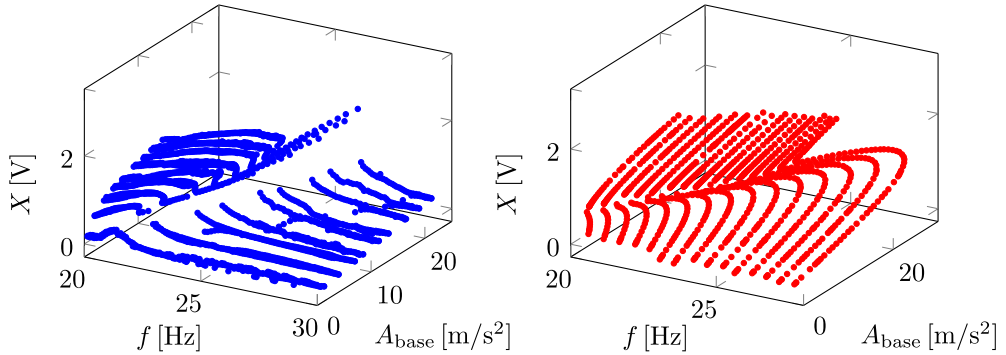


Figure 1: Frequency sweeps (left panel), and control-based continuation (right panel).

which would otherwise remain undetectable, providing a more robust basis for model building and parameter identification.

2. Motivation

In case of nonlinear structures, it is a common approach to use the frequency response to characterise the system, see e.g. [1, 32]. This response is often measured in a forced or base-excitation setting, by performing two frequency sweeps, one with increasing and another with decreasing forcing frequency. Thus, in principle, every stable solutions can be captured even in bistable frequency domains. With the help of frequency-sweeps, performed at different forcing amplitudes, one can trace the stable part of the response surface in the forcing frequency – forcing amplitude parameter plane.

An example is shown in the left panel of Fig. 1 with the response surface of the vibration amplitudes X for the nonlinear oscillator, described in Section 3. It can be observed that, while the frequency-sweeps were performed at constant shaker voltage amplitude due to the internal dynamics of the shaker, the shaker acceleration amplitude A_{base} varies slightly during each sweep. We traced the same surface by performing control-based continuation at constant frequencies (see the right panel). This method is not only capable of capturing the unstable solutions but the feedback control on the periodic solution also results in a smoother response surface.

If the measurements are contaminated with noise, it can be challenging to trace steady-state solutions in parameter ranges where the system undergoes bistable behaviour. This bistable behaviour is typically characterised by the presence of three solution branches within the same parameter range, where

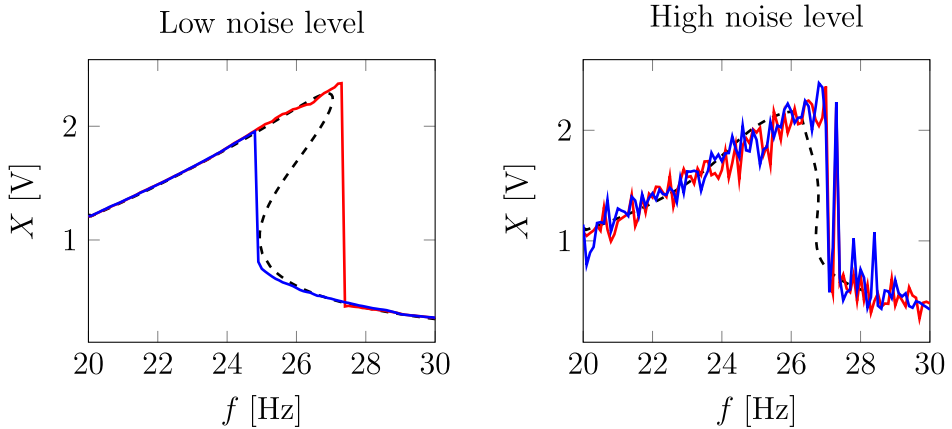


Figure 2: Comparison of frequency sweeps (red and blue curves) in case of low and high levels of measurement noise. A seventh-order duffing-like oscillator best fit is indicated by the dashed black curves.

two solution branches are connected by an unstable branch through saddle-node bifurcations. If parameter sweeps are performed, in addition to the lack of information regarding the unstable solutions, one may erroneously observe that the vibration amplitude jumps earlier than the saddle-node bifurcations are located in the solution branch of the underlying noise-free system. Ultimately, this leads to a loss of information not only about the unstable branch but also parts of the stable solution branches. Moreover, it may not be possible to identify a clear fold point in the captured solution manifold as the noise may cause the system to jump repeatedly between the domains of attraction of two steady-state solutions [2].

This phenomenon is illustrated by the example in Fig. 2 where two frequency sweeps, carried out on the nonlinear oscillator, are compared. In both cases, the oscillator was modelled as a seventh-order Duffing-like oscillator fitted to the frequency response. The response of the fitted model is indicated by the black curves. It can be seen that in the low noise case, in spite of not having information about the unstable solutions, the fitted mathematical model matches with the measured vibration amplitudes reasonably well. However, with higher levels of noise, the bistable domain is not properly traced and the fitted model provides an entirely different response to that using the low-noise data.

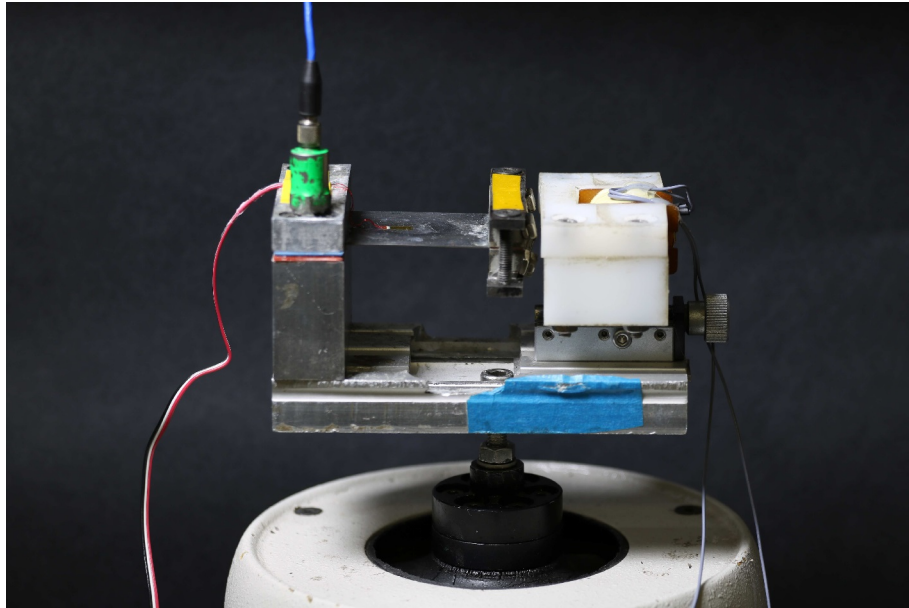


Figure 3: The experimental setup: a nonlinear oscillator mounted on the shaker.

3. The experimental rig

In our study, we investigate the properties of the forced nonlinear oscillator shown in Fig. 3. This device is designed to show nonlinear behaviour to make it suitable to test the capabilities of experimental algorithms [4, 5], while in former studies, it was also used as an energy harvester [8]. The structure of the device is shown in Fig. 4. The nonlinear oscillator is formed from a thin steel plate, which is clamped to the base as a cantilever beam. This clamp includes plastic plates supporting the steel plate to add damping to the contact. At the other end, two iron masses, incorporating four permanent magnets, are attached to the tip of the plate. The orientation of the poles of these magnets is indicated by the red arrows in Fig. 4. The resultant magnetic field interacts with a stator (see the white block in Fig. 3), which consists of an electromagnetic coil with an iron core in an insulated housing.

The rigid base of the oscillator and the stator is mounted on a shaker, providing forcing to the system. As the plate vibrates, the magnets at the free end will move relative to the coil changing the magnetic flux. The resulting combination of structural, inertial, and magnetic forces results in

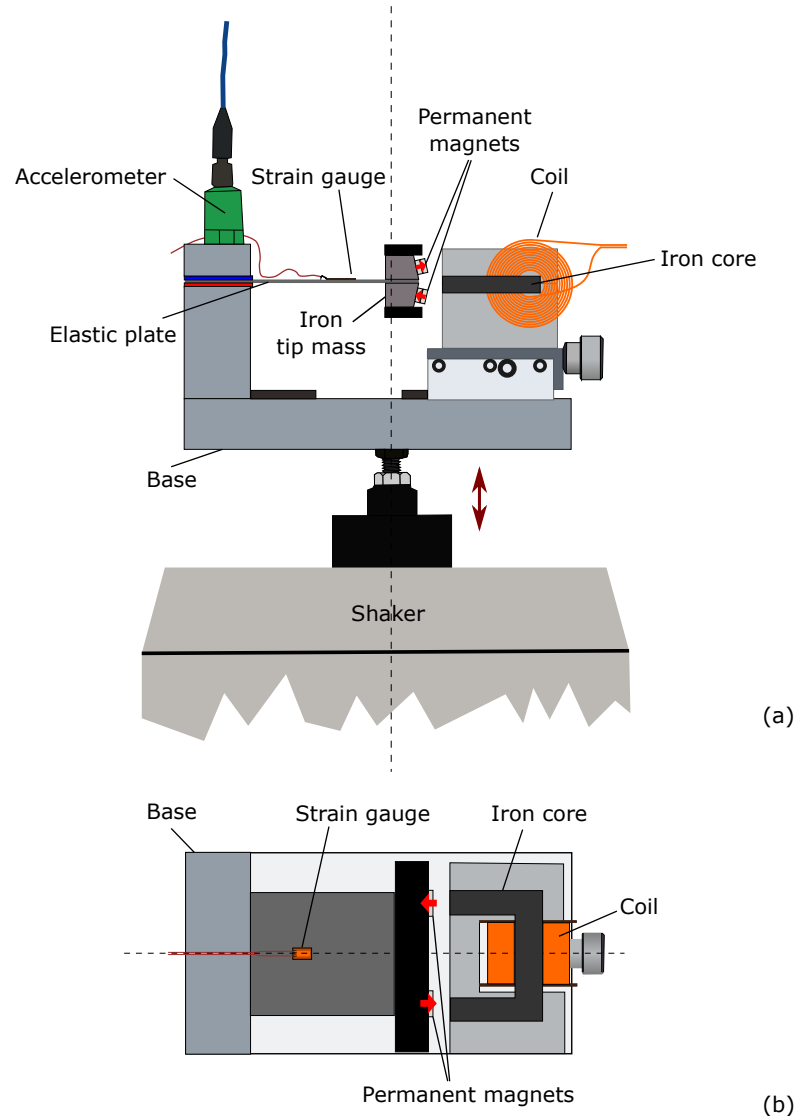


Figure 4: The experimental rig: schematics of the nonlinear oscillator on a shaker. Panel (a): top view, panel (b) side view. For visibility of the coil and its core, their housing is shown in the background only.

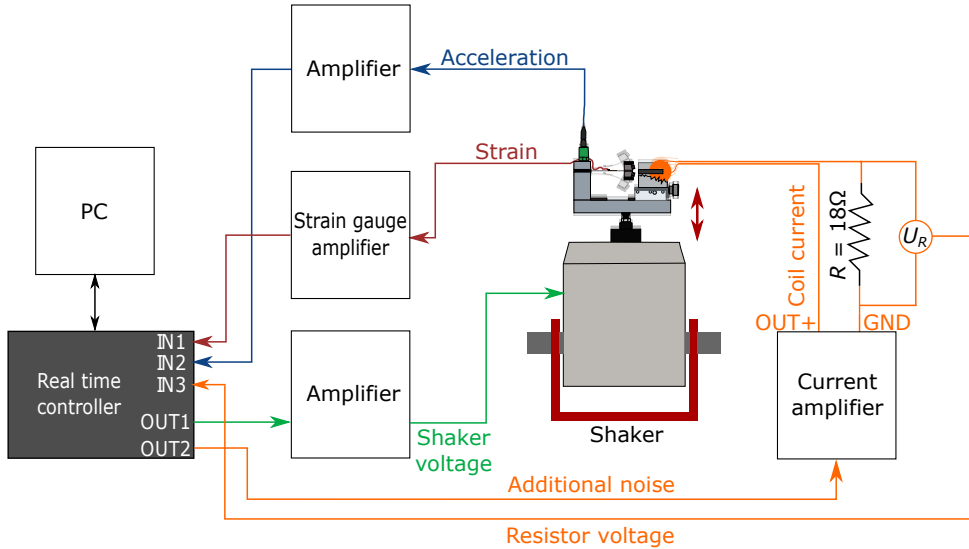


Figure 5: The experimental rig: schematics of the experimental setup for control and data acquisition.

a nonlinear restoring force. According to Faraday's law of electromagnetic induction, the changing magnetic flux also generates an electromotive force, which can be measured as a changing voltage across the coil. Similarly, a current flowing through the coil results in a magnetic flux and so generates a magnetic force, which allows the excitation of the system through the coil. In our experiments, we used the coil to pollute the experiment with additional noise.

Figure 5 shows a schematic of the experimental set up including data acquisition and control. The data acquisition and demand generation is carried out by a real-time controller box built upon a BeagleBone Black board [3]. Three input and two output voltage signals are handled by the real-time controller. The demand voltage OUT1 is applied to the shaker using an amplifier while the demand OUT2 is used to contaminate the experiment with noise. For this purpose, we use a current amplifier to regulate the current flowing through the coil according to the noisy signal generated by the controller box.

The vibration of the elastic plate is measured using a strain-gauge, which is connected to an amplifier in a quarter-bridge configuration. The voltage, provided by the strain-gauge amplifier, is measured at the acquisition channel

IN1. Channel IN2 is connected to an accelerometer that is mounted on the top of the base of the nonlinear oscillator, while IN3 records voltage that is generated across a resistor by the current flowing through the coil (see the circuit in Fig. 5).

While the control is real time, the continuation algorithm and the setting of new control targets in the controller is not real time. Therefore, these tasks were carried out by a PC, which was also used to process the acquired data.

4. Control-based continuation

We employ the technique of control-based continuation to determine the response of the nonlinear oscillator to periodic forcing. Let us consider a one-degree-of-freedom forced nonlinear system as a model of the experimental rig in the form of

$$\ddot{x} + g(\dot{x}, x) = F(t), \quad (1)$$

where the state variable x is the input voltage from the strain-gauge (IN1), the dot refers to differentiation with respect to time, the function g contains all the nonlinearities, while $F(t)$ corresponds to the forcing provided by the shaker. Despite the fact that this model does not include the electromagnetic effects in the system explicitly, we found that the one-degree-of-freedom model can characterise the response to periodic forcing with good accuracy. Note, that, as demonstrated in [7], this is not the case for non-periodic excitation.

The forcing $F(t)$ is composed by two parts: a periodic component and an additional control term F_{ctrl}

$$F(t) = A \cos(\omega t) + B \sin(\omega t) + F_{\text{ctrl}}, \quad (2)$$

where ω is the angular frequency of the forcing whereas A and B are constant coefficients. To capture the nonlinear response of the open-loop (uncontrolled) system, the control has to fulfil two conditions: it has to be stabilising and non-invasive, i.e. the steady-state response of the controlled system has to be equal to the steady-state response of the open-loop system. This is ensured by the proportional-derivative control law given in the form

$$F_{\text{ctrl}} = k_p(x^* - x) + k_d(\dot{x}^* - \dot{x}), \quad (3)$$

where x^* is the control target while k_p and k_d are the proportional and derivative control gains.

In the control algorithm, both the desired and measured strain-gauge voltages are represented by their truncated Fourier series

$$x(t) \approx \frac{A_0}{2} + \sum_{k=1}^N (A_k \cos(k\omega t) + B_k \sin(k\omega t)), \quad (4)$$

$$x^*(t) \approx \frac{A_0^*}{2} + \sum_{k=1}^N (A_k^* \cos(k\omega t) + B_k^* \sin(k\omega t)). \quad (5)$$

In our test, the first seven harmonics were retained ($N = 7$).

As a result, the total forcing $F(t)$ also can be expressed in a similar form

$$F(t) = \frac{A_{F0}}{2} + \sum_{k=1}^N (A_{Fk} \cos(k\omega t) + B_{Fk} \sin(k\omega t)), \quad (6)$$

where the coefficients are given by

$$A_{F1} = A + k_p(A_1^* - A_1) - k_d\omega(B_1^* - B_1), \quad (7a)$$

$$B_{F1} = B + k_p(B_1^* - B_1) + k_d\omega(A_1^* - A_1), \quad (7b)$$

$$A_{Fk} = k_p(A_k^* - A_k) - k_dk\omega(B_k^* - B_k) \text{ for } k = 0, 2, 3, \dots, N, \quad (7c)$$

$$B_{Fk} = k_p(B_k^* - B_k) + k_dk\omega(A_k^* - A_k) \text{ for } k = 2, 3, \dots, N. \quad (7d)$$

Studying the expressions (7a) and (7b) reveals that the fundamental harmonic component of the total forcing $\Phi = \sqrt{A_{F1}^2 + B_{F1}^2}$ is not fully determined by the open-loop forcing coefficients A and B , as it also depends on the control target $x^*(t)$ and the response $x(t)$. Moreover, the control introduces higher-harmonic components to the total forcing that have to be eliminated to capture the response of the open-loop system.

In our study, control-based continuation is used to generate the family of steady-state solutions of the system across a range of the forcing amplitudes while keeping the forcing frequency constant. Since, in this case, a unique forcing amplitude corresponds to every the vibration amplitude, it is possible to trace the whole branch of solutions by a sweep in the target fundamental harmonic amplitude B_1^* , with keeping $A_1^* = 0$ to fix the phase of the response. This means that there is a linear relationship between the

continuation parameter and the forcing $F(t)$, which enables us to use a simplified version of the ‘full’ continuation algorithm (see [31] for example). The simplified control-based continuation algorithm is briefly described below — a full description is given in [27].

Let us assume that the experiment is running at a steady-state given by the target coefficients $(A_{F1}^j, B_{F1}^j, A_0^{*j}, B_1^{*j}, A_k^{*j}, B_k^{*j})^j$, $k = 2, \dots, N$, with $A_1^{*j} = 0$. Then, to find the next point in the solution branch, the fundamental harmonic coefficient of the control target is increased $B_1^{*j+1} := B_1^{*j} + \Delta$. After waiting for the control to reach steady-state, if necessary, we apply fixed point iteration to correct the higher-harmonic coefficients of the control-target until coefficients corresponding to the higher harmonics of the forcing $(A_{Fk}, B_{Fk}, k = 0, 2, 3, \dots, N)$ are below a pre-defined tolerance. Once the higher harmonics in the forcing are eliminated, the actual state, given by $(A_0^{*j+1}, B_1^{*j+1}, A_k^{*j+1}, B_k^{*j+1})^{j+1}$, $k = 2, \dots, N$, is accepted as the steady-state response of the open loop system corresponding to the forcing amplitude $\Phi^{j+1} = \sqrt{A_{F1}^{2(j+1)} + B_{F1}^{2(j+1)}}$.

Provided that appropriately chosen control gains are used, this algorithm ensures a stable, non-invasive control, which traces the solution branch sweeping across the vibration amplitudes. A possible alternative could be to use a secant prediction to provide an initial guess for the algorithm in the direction obtained from the previous two points on the branch. This method may result in the algorithm reaching a fixed point in fewer iteration steps in an experiment with low noise; however, the amplitude sweep is more robust against noise since with this assumption, noise cannot affect the direction along the branch in which the next branch point is predicted which is an effect that can hinder progress along a branch. A further advantage is that the correction of the solution is carried out in a derivative-free way. Thus, it requires less evaluation at each iteration step, leading to faster convergence.

4.1. Model of the nonlinear oscillator

We use the experimentally acquired bifurcation diagrams to identify the parameters of our model for the experimental rig, the one-degree-of-freedom nonlinear oscillator (see Eq. (1)). We consider a linearly damped, Duffing-like oscillator with the equation of motion

$$\ddot{x} + b\dot{x} + \omega_n^2 x + \mu x^3 + \nu x^5 + \rho x^7 = \delta_{st}\omega_n^2 \cos(\omega t), \quad (8)$$

where ω_n is the linear natural angular frequency, δ_{st} is the equivalent static deflection for the forcing amplitude $\delta_{st}\omega_n^2$, while the damping is given by the

parameter b , whereas μ , ν and ρ characterise the nonlinearities in the system. We consider the odd nonlinear terms up to seventh order as this proved to be satisfactory to characterise the experimental rig.

The fundamental harmonic component of the steady-state system response can be given as $X \cos(\omega t + \vartheta)$ with amplitude X and phase angle ϑ . Using the method of multiple scales [22], an analytical approximate solution can be obtained for the fundamental harmonic component. Based on this, for a given vibration amplitude X , the phase angle and the static deflection can be given as

$$\vartheta = \arctan \left(\frac{\tilde{b}\zeta}{(\zeta^2 - 1) - \frac{35}{64}X^6\tilde{\rho} - \frac{5}{8}X^4\tilde{\nu} - \frac{3}{4}X^2\tilde{\mu}} \right), \quad (9)$$

$$\delta_{\text{st}} = \left| \frac{\frac{35}{64}X^7\tilde{\rho} + \frac{5}{8}X^5\tilde{\nu} + \frac{3}{4}X^3\tilde{\mu} - X(\zeta^2 - 1)}{\cos(\vartheta)} \right|, \quad (10)$$

with $\zeta = \omega/\omega_n$, $\tilde{b} := b/\omega_n$, $\tilde{\mu} := \mu/\omega_n^2$, $\tilde{\nu} := \nu/\omega_n^2$, $\tilde{\rho} := \rho/\omega_n^2$. The derivation of these formulae is given in the appendix.

Substituting (9) into Eq. (10), we obtain the static deflection by means of the system and forcing parameters as well as the amplitude of the fundamental harmonic component of the steady-state response

$$\delta_{\text{st}} = \delta_{\text{st}}(X, \tilde{\mu}, \tilde{\nu}, \tilde{\rho}, \tilde{b}, \zeta). \quad (11)$$

4.2. Numerical collocation

It has to be noted that the solution presented above is only accurate for ‘weakly nonlinear’ systems where the nonlinear terms do not dominate over the underlying linear system. To check the accuracy of the approximate solution we carried out the numerical continuation of the periodic solutions in (8). The results are compared in Fig. 6 for the parameters $\mu = 1.499$, $\nu = -0.3921$, $\rho = 0.0422$, $b = 0.3159$ and $f_n = 19.95$ Hz. Both frequency and amplitude variation is checked. The results indicate that the analytical approximation provides very accurate results in the parameter-range of our interest.

5. Parameter identification

We use the expression in Eq. (11) to identify the system parameters by fitting it to measurement results, based on least square errors. However, the

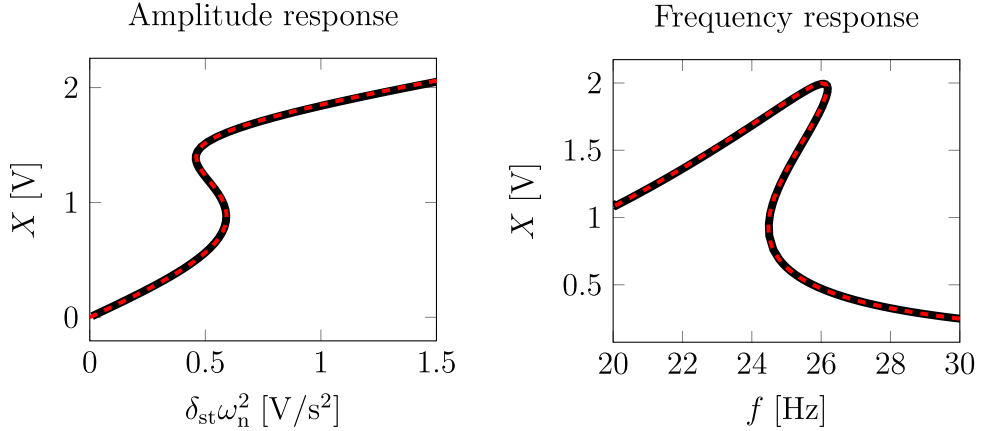


Figure 6: Comparison of the analytical approximate, and numerical solutions of Eq. (8). In the left panel, the forcing frequency is kept constant $f = 24$ Hz while the excitation amplitude is varied. In the right panel, the frequency response is shown for a constant forcing amplitude of $\delta_{st}\omega_n^2 = 0.7$ V/s².

amplitude $\delta_{st}\omega_n^2$ of the forcing provided by the shaker is not measured directly. Instead, we capture the acceleration a_{base} of the base of the oscillator. We assume that the base acceleration and forcing are proportional: $\delta_{st} = c_A A_{base}$, where A_{base} is the fundamental harmonic amplitude of the base acceleration. This leads to an expression for the base acceleration amplitude that can be directly used for parameter identification

$$A_{base} = c_A \delta_{st}(X, \tilde{\mu}, \tilde{\nu}, \tilde{\rho}, \tilde{b}, \zeta). \quad (12)$$

Note that the base acceleration is not controlled directly in the experiment as the real time controller sets the shaker voltage instead. In Eq. (12), the frequency ratio ζ is set by the user (provided the natural angular frequency ω_n is a priori determined) whereas the response amplitude X is measured. Consequently, we aim to identify the parameters \tilde{b} , $\tilde{\mu}$, $\tilde{\nu}$, $\tilde{\rho}$ and c_A such that they minimise the least square error based on Eq. (12). Assuming that m measurement points, given by $(A_{basei}, \zeta_i, X_i)$, are acquired, the function to be minimised can be expressed as

$$R = \sum_{i=1}^m \left(A_{basei} - c_A \delta_{st}(X_i, \tilde{\mu}, \tilde{\nu}, \tilde{\rho}, \tilde{b}, \zeta_i) \right)^2. \quad (13)$$

The least square fit is obtained by using the gradient-free principal-axis method of the NLOpt package in Julia [13]. Once the least square fit is per-

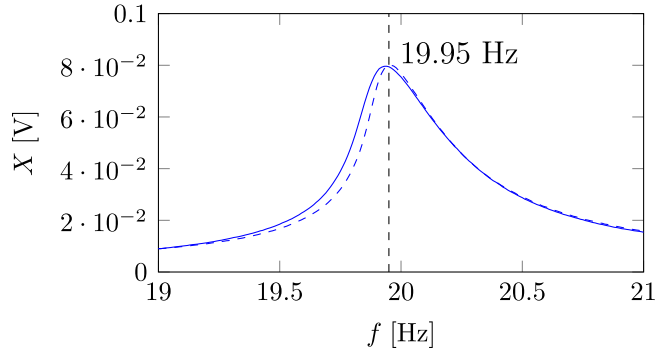


Figure 7: Linear frequency response: up-sweep (blue continuous), down-sweep (blue, dashed)

formed, the original model parameters $b = \tilde{b}\omega_n$, $\mu = \tilde{\mu}\omega_n^2$, $\nu = \tilde{\nu}\omega_n^2$, $\rho = \tilde{\rho}\omega_n^2$ can be recovered.

6. Effect of noise on parameter identification

6.1. Underlying linear response

The measurement procedure is as follows. Firstly, the linear frequency response of the system is extracted by performing an open-loop frequency sweep with a low shaker voltage amplitude ($U_{\text{shaker}} = 0.01$ V) where the effect of the nonlinearities is marginal. We performed an up and a down-sweep between 19-21 Hz with an increment of 0.1 Hz (see Fig. 7). One can observe a slight discrepancy between the two curves which can be explained by the effect of temperature change during the measurement. Estimating the damping with the 3 dB bandwidth method indicated that, at this level of excitation, the Lehr's damping ratio of the system is below 0.01. This means that the difference between the measurable ‘damped’ and the undamped natural frequencies is below 0.01%. Therefore, we accepted the locus of the maximum of a response curve as the undamped natural frequency. Since the up- and down-sweeps provided different results, we calculate with the average of the two peaks $f_n = 19.95$ Hz as the natural frequency of the system.

6.2. Robustness of solution tracing methods against noise

The core of our study was to assess the performance of control-based continuation against open-loop parameter-sweeps in scenarios where the experiment was polluted with different levels of noise. We used the real-time

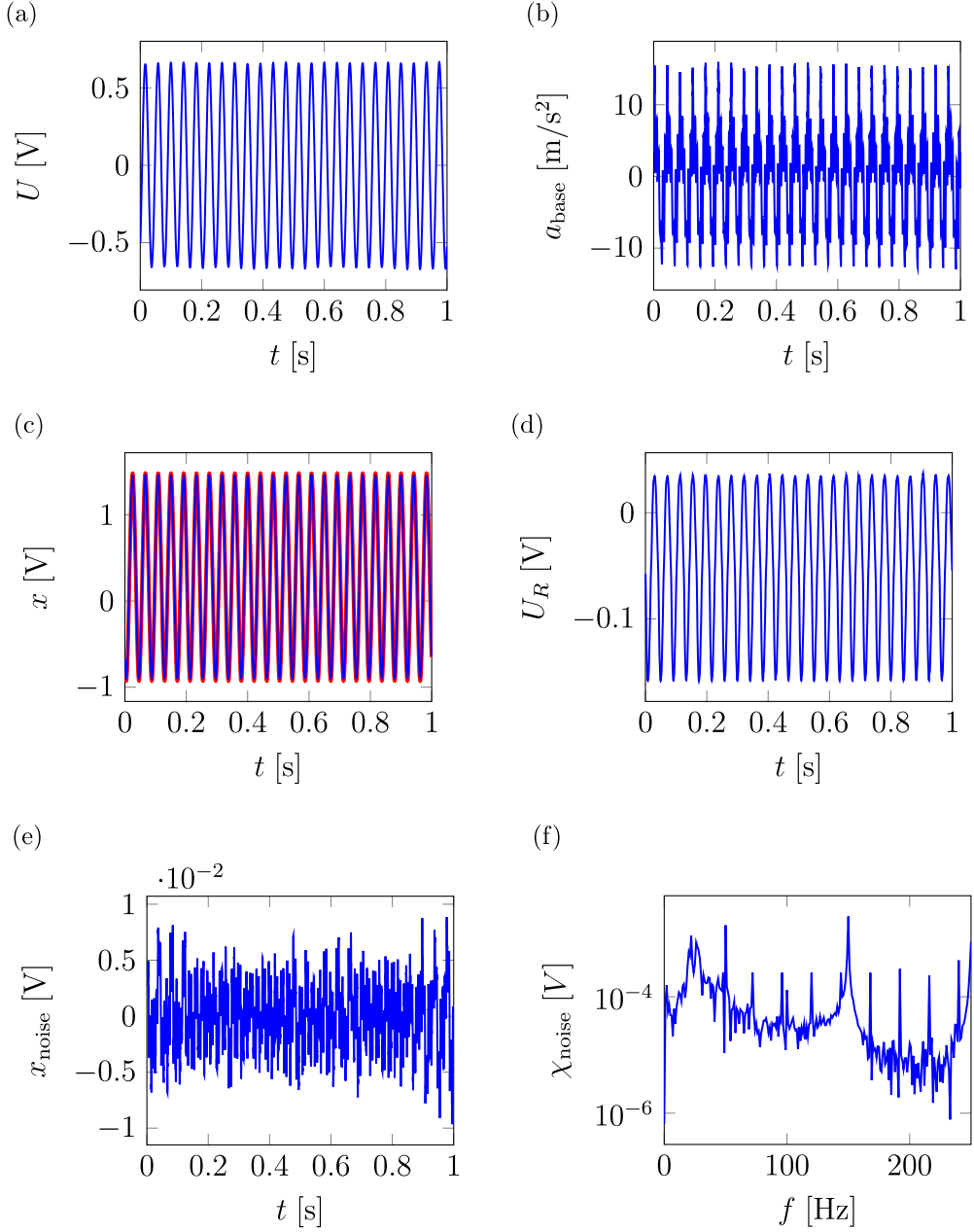


Figure 8: Acquired data and outputs generated by the real time controller at low noise-level. (a) shaker voltage U , (b) base acceleration a_{base} , (c) target (red) and actual (blue) strain-gauge voltage x , (d) resistor voltage U_R , (e) noise time profile x_{noise} , (f) noise FFT χ_{noise} .

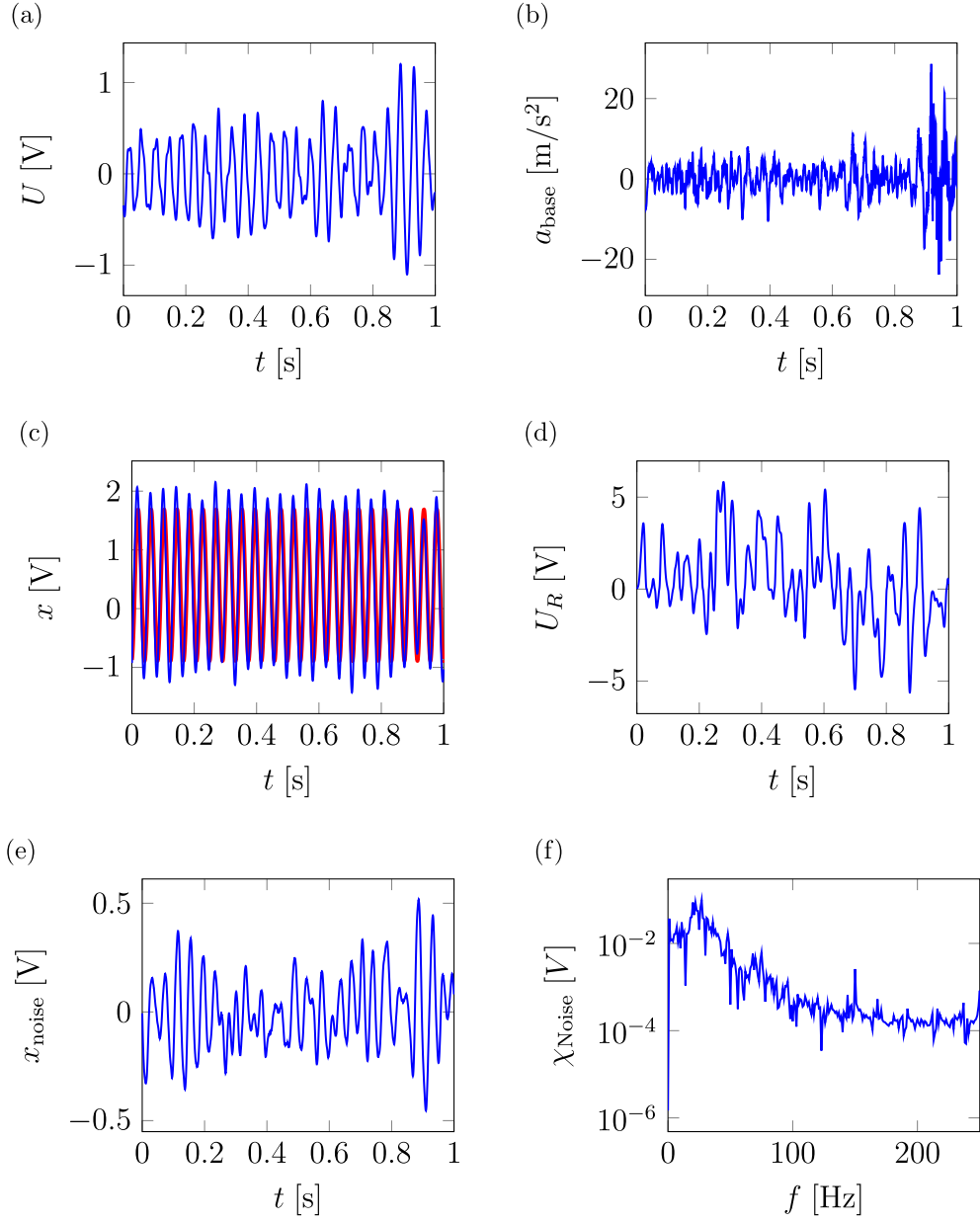


Figure 9: Acquired data and outputs generated by the real time controller at high noise-level (N10). (a) shaker voltage U , (b) base acceleration a_{base} , (c) target (red) and actual (blue) strain-gauge voltage x , (d) resistor voltage U_R , (e) noise time profile x_{noise} , (f) noise FFT χ_{noise} .

controller generate a random demand for the current flowing through the electromagnetic coil by generating a series of pseudo-random numbers and feeding the signal through a low-pass Butterworth filter resulting in a band-limited noise with a cutoff frequency of 50 Hz [3]. Time profiles of the input and output signals, without and with additional noise, are shown in Fig. 8 and 9 respectively. The noise x_{noise} in these diagrams is obtained by subtracting the harmonic components of the strain-gauge voltage x , identified by the real-time controller.

In the case where no noise is added through the coil, see Fig. 8, other uncontrolled noise sources provide a low noise-level of below 1% of the vibration amplitude. The notable peaks in the noise FFT belong to the power supply frequency and its upper harmonics (50, 100, 150 Hz) while one can also observe smaller peaks ($n \times 24$ [Hz]) related to numerical errors in the calculation of the harmonic coefficients. These components become negligible when significant noise is added to the system through the coil, resulting in more evenly distributed frequency components as shown in Fig. 9.

While the control is clearly affected by the added noise, the algorithm is still capable to stabilise the system around the periodic solutions of the underlying noise-free system even when the noise amplitude is about 30% of the vibration amplitude.

Also note how the presence of noise affects the current in the coil (measured through the voltage on a resistor): if there is no additional noise in the system, the coil current appears to be largely harmonic, as its main source is electromagnetic induction due to the tip mass passing the iron core. This component practically disappears in the additional noise.

Using control-based continuation in a noise-polluted environment is more challenging as error tolerances are more difficult to meet. Moreover, if a secant predictor is used, as is common with the pseudo-arc length method, the algorithm may fail resulting in repeated, or to the contrary, no coverage of some parts of the solution manifold. These challenges were addressed in [28] with techniques developed specifically to cope with noise.

In our case though, it proved to be sufficient to adjust the simplified control-based continuation algorithm by averaging the coefficients of 10 periods and allowing a higher error tolerance in the noisy measurements. In some cases though, even increased tolerances were difficult to meet; therefore, at higher noise levels we omitted the step of the algorithm that corrects the higher harmonics and accepting the solution we obtained by simply changing the fundamental harmonic component of the control target. It is worth

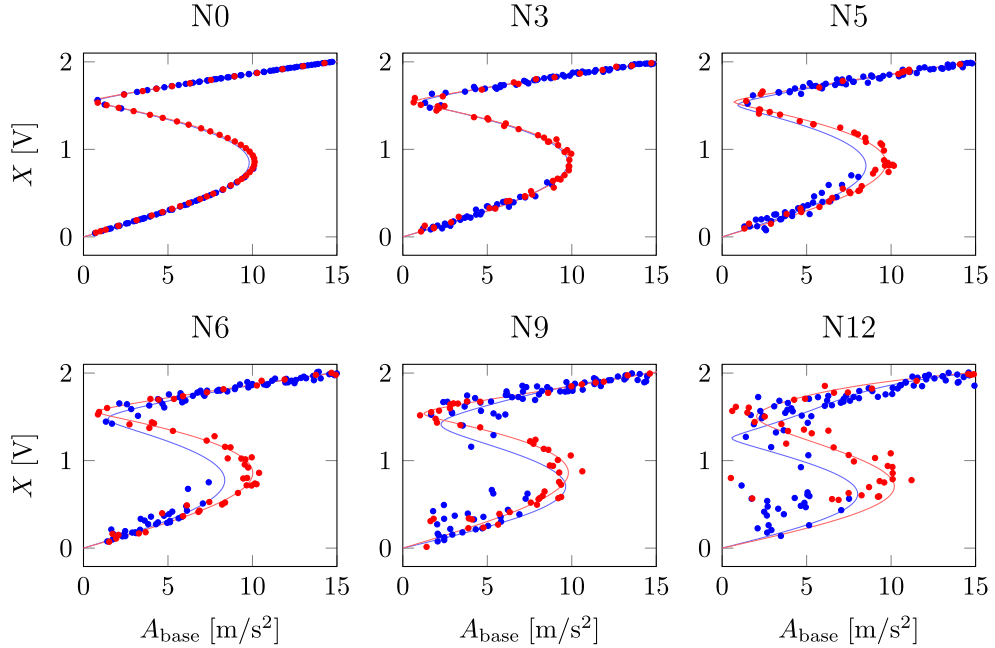


Figure 10: Amplitude response of the nonlinear oscillator at 24 Hz, at different noise levels. The markers show the measurement data while the response of the fitted surrogate model is indicated by the continuous lines. The blue markers and curves belong to parameter-sweeps while the red ones to CBC.

mentioning that this is always the case in the open-loop measurements when steady-state solutions are accepted without any correction step.

We also used the fact that, due to the choice of continuation in amplitude (rather than frequency), a unique solution exists for every response amplitude. Thus, performing a sweep in the targeted vibration amplitudes ensured that the continuation of the solution branch did not stall and the whole branch was covered.

In Fig. 10, we compared control-based continuation and open-loop forcing amplitude sweeps under different levels of noise load. The labels beginning with N indicate the magnitude of noise we added through the coil, e.g. N3 means that the noise magnitude is three times as the reference N1 while N0 corresponds to the case when the experiment was not polluted with noise through the coil.

In the top row of panels of Fig. 10, we show the measurements where we had a maximum tolerance for the higher harmonics in the control-based

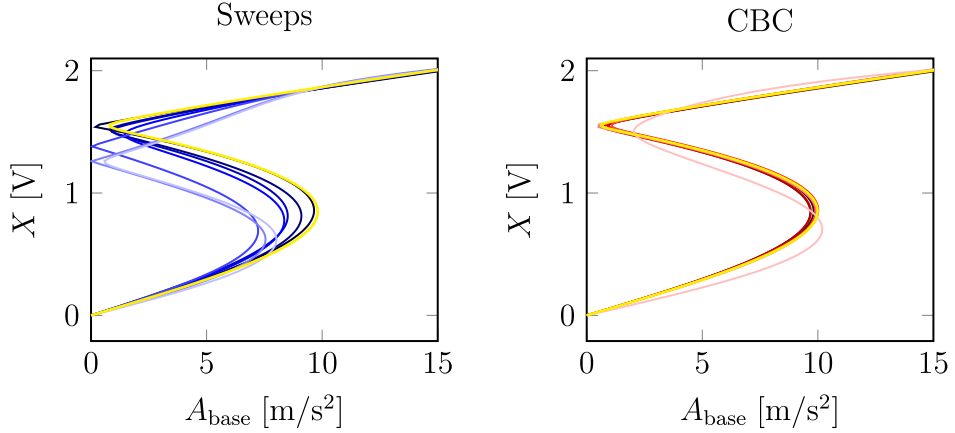


Figure 11: Robustness against noise: The amplitude responses fitted to amplitude sweeps (left panel) and control based continuation (right panel) with base acceleration. The curves belong to noise-levels N2, N4, N5, N6, N8, N10 and N12 with higher noise indicated by lighter shading. The response-curves belonging to the cases without additional noise (N0) are highlighted in yellow.

continuation algorithm whereas in the measurements shown in the bottom row, we accepted the result without introducing corrections to the higher harmonic components. Comparing the cases N5 and N6 which were performed with a similar amount of noise but one with, and the other without higher harmonic control, we can see that we did not introduce significant further error in the experiment by not setting a maximum tolerance at higher noise levels.

It can be observed that if the experiment is running with a low amount of noise (see N3) both methods, the standard open-loop sweep and control-based continuation provide a response close to the case with no additional noise (N0), which we take to be the baseline ‘correct’ solution. However, at medium noise levels (see N5, N6 and N9) the jumps in the open-loop data between the low and high amplitude parts of the solution branch occur significantly earlier than the folds in the branch of steady-state solutions of the underlying noise-free system. Meanwhile, control-based continuation is still able to trace the entire family of solutions and to retain the response curve of the low noise system with reasonable accuracy. This is true even at high noise level (see N12) to some extent — even though control-based continuation begins to struggle in tracking the branch, it still provides some information about the unstable solutions while the bistable region cannot be

Open-loop measurements					
Noise	$\hat{\mu}$	$\hat{\nu}$	$\hat{\rho}$	\hat{b}	c_U
N0	0.299736	-0.0230188	-0.000545094	0.0130789	0.0266871
N2	0.303894	-0.0267741	-8.27812e-7	1.46088e-7	0.0259024
N3	0.304695	-0.027294	-6.7781e-5	0.014032	0.0276606
N4	0.34947	-0.0555996	0.00423664	0.011461	0.0257957
N5	0.346713	-0.0525806	0.00401672	0.0217511	0.0266217
N6	0.398974	-0.0866717	0.00885885	0.0217511	0.0266217
N8	0.516524	-0.163626	0.0209883	1.81859e-10	0.0271741
N9	0.506837	-0.160171	0.0193367	0.0274644	0.0207488
N10	0.636571	-0.241319	0.0319608	4.9275e-9	0.0234011
N12	0.644793	-0.248782	0.0331903	0.00830185	0.0219059

Control-based continuation					
Noise	$\hat{\mu}$	$\hat{\nu}$	$\hat{\rho}$	\hat{b}	c_U
N0*	0.29995	-0.0257753	-0.000252701	0.0079761	0.0249586
N2*	0.298945	-0.0233512	-0.000669121	0.010041	0.0253846
N3*	0.292901	-0.0185704	-0.00157755	0.0101766	0.0253763
N4*	0.313156	-0.0344051	0.00113597	0.0121747	0.0253811
N5*	0.305511	-0.0269727	-0.000312632	0.00969982	0.0254893
N6†	0.291671	-0.0206321	-0.00101879	0.0112381	0.0251575
N8†	0.303191	-0.027599	-0.000102184	0.0142532	0.0251187
N9†	0.275549	-0.00172186	-0.0049329	0.0175988	0.0260507
N10†	0.315962	-0.0365078	0.00129476	-0.00577997	0.0246026
N12†	0.521444	-0.188949	0.0260422	0.0218853	0.0194733

Table 1: The identified model parameters with open-loop amplitude-sweeps and control-based continuation at different noise levels: the coefficients $\hat{\mu}$, $\hat{\nu}$, $\hat{\rho}$ of the 3rd, 5th and 7th order terms, the linear viscous damping \hat{b} and the scaling factor c_U between the forcing and base acceleration. In case of the control-based continuation data, the symbols * and † refer to measurements with and without a maximum tolerance for the higher harmonic components of the forcing, respectively.

recovered by parameter sweeps.

This can be well demonstrated by Fig. 11 where we compare the response curves obtained by fitting the parameters of the seventh-order Duffing-like oscillator, given by Eq. (8), to measurement results acquired at different noise levels. The identified model parameters are listed in Table 1 for both set of measurements, the amplitude-sweeps and control-based continuation, respectively. From these results, it is clear that control-based continuation is able to preserve the original response curve better than frequency sweeps.

7. Conclusions

By investigating the steady-state response of a forced nonlinear oscillator under different levels of noise, the robustness of control-based continuation was assessed by comparing it to open-loop measurements.

Based on the acquired data, we carried out parameter identification of a seventh-order Duffing-like oscillator to quantify and characterise the performance of the two solution tracking methods. We demonstrated that the ability of control-based continuation to capture both stable and unstable periodic solutions, and the fact that we have feedback control on the response, result in a more robust coverage of the solution branch than in case of parameter-sweeps. Furthermore, while an open-loop parameter sweep can perform as well as control-based continuation at low noise levels, it has a tendency to miss parts of the stable solutions in bistable parameter domains as the additional noise can cause the system to jump between the domains of attraction of the co-existing stable solutions. This can result in poorly identified parameters in the model, while fitting the model to data obtained by control-based continuation yields a response-curve that is closer to the response of the underlying noise-free system.

As control-based continuation is affected by noise, albeit to a lesser degree, it is still an open question to what extent can one expect recover the response of the underlying deterministic system in a heavily noise-contaminated measurement. In general, control-based continuation is capable to extract more information from experiments than open-loop measurements. Thus, with the help of control-based continuation it may be possible to capture finer, otherwise undetectable, details about the dynamics of physical systems.

Data statement

All the experimental data used in this paper have been deposited into the University of Bristol Research Data Repository and is publicly available for download.

Acknowledgements

This research has received funding from the *Next-generation test methods for nonlinear structures* (EP/P019323/1) and the *Digital twins for improved dynamic design* (EP/R006768/1) EPSRC grants. The support of the EPSRC is greatly acknowledged.

References

- [1] V. Agarwal, X. Zheng, and B. Balachandran. Influence of noise on frequency responses of softening Duffing oscillators. *Physics Letters, Section A: General, Atomic and Solid State Physics*, 382(46):3355–3364, nov 2018. ISSN 03759601. doi: 10.1016/j.physleta.2018.09.008.
- [2] D. Barkley, I.G. Kevrekidis, and A.M. Stuart. The Moment Map: Nonlinear Dynamics of Density Evolution via a Few Moments. *SIAM Journal on Applied Dynamical Systems*, 5(3):403–434, 2006.
- [3] D.A.W. Barton. A real-time controller (RTC) based on the Beagle Bone Black. <https://github.com/dawbarton/rtc>, 2015. [Open-source].
- [4] D.A.W. Barton and S.G. Burrow. Numerical Continuation in a Physical Experiment: Investigation of a Nonlinear Energy Harvester. *Journal of Computational and Nonlinear Dynamics*, 6(1):011010, 2011. ISSN 15551423. doi: 10.1115/1.4002380.
- [5] D.A.W. Barton, B.P. Mann, and S.G. Burrow. Control-based continuation for investigating nonlinear experiments. *JVC/Journal of Vibration and Control*, 18(4):509–520, apr 2012. ISSN 10775463. doi: 10.1177/1077546310384004.
- [6] G.I. Bischi, C. Chiarella, and L. Gardini. *Nonlinear Dynamics in Economics, Finance and the Social Sciences*. Springer-Verlag, Berlin Heidelberg, 1 edition, 2010.

- [7] A. Cammarano. *Increasing the Bandwidth of Resonant Vibration-Based Energy Harvesters*. PhD thesis, University of Bristol, 2012.
- [8] A. Cammarano, S.G. Burrow, and D.A.W. Barton. Modelling and experimental characterization of an energy harvester with bi-stable compliance characteristics. *Proceedings of the Institution of Mechanical Engineers. Part I: Journal of Systems and Control Engineering*, 225(4): 475–484, jun 2011. ISSN 0959651811403093. doi: 10.1177/0959651811403093.
- [9] M. Feldman. Time-varying vibration decomposition and analysis based on the hilbert transform. *Journal of Sound and Vibration*, 295:518–530, 2006.
- [10] S.K. Goharoodi, K. Dekemele, L. Dupre, M. Loccufer, and G. Crevecoeur. Sparse Identification of Nonlinear Duffing Oscillator From Measurement Data. apr 2018.
- [11] J. Guckenheimer and P.J. Holmes. *Nonlinear Oscillations, Dynamical Systems and Bifurcations of Vector Fields*. Springer-Verlag, New York, 1 edition, 1983.
- [12] N.B. Janson. Non-linear dynamics of biological systems. *Contemporary Physics*, 53:137–167, 2012.
- [13] S.G. Johnson. The NLopt module for Julia (version 2.5.0). <https://github.com/JuliaOpt/NLopt.jl>, 2018. [Open-source].
- [14] G. Kerschen, K. Worden, A.F. Vakakis, and J.C. Golinval. Past, present and future of nonlinear system identification in structural dynamics. *Mechanical Systems and Signal Processing*, 20:505 – 592, 2006.
- [15] Y. Kuzentsov. *Elements of Applied Bifurcation Theory*. Springer-Verlag, New York, 2004.
- [16] W. Lacarbonara, B. Balachandran, J. Ma, J.A. Teneiro Machado, and G. Stepan. *Nonlinear Dynamics of Structures, Systems and Devices*. Springer International Publishing, 1 edition, 2020.
- [17] I.J. Leontaritis and S.A. Billings. Input-output parametric models for nonlinear systems, part i: deterministic nonlinear systems. *International Journal of Control*, 41:303328, 1985.

- [18] I.J. Leontaritis and S.A. Billings. Input-output parametric models for nonlinear systems, part ii: stochastic nonlinear systems. *International Journal of Control*, 41:329344, 1985.
- [19] S. Marchesiello and L. Garibaldi. A time domain approach for identifying nonlinear vibrating structures by subspace methods. *Mechanical Systems and Signal Processing*, 22(1):81–101, jan 2008. ISSN 08883270. doi: 10.1016/j.ymssp.2007.04.002.
- [20] S.F. Masri, J.P. Caffrey, T.K. Caughey, A.W. Smyth, and A.G. Chassiakos. Identification of the state equation in complex non-linear systems. *International Journal of Non-Linear Mechanics*, 39(7):1111–1127, sep 2004. ISSN 00207462. doi: 10.1016/S0020-7462(03)00109-4.
- [21] M.D. Narayanan, S. Narayanan, and C. Padmanabhan. Parametric Identification of a Nonlinear System Using Multi-harmonic Excitation. Technical report.
- [22] A.H. Nayfeh. *Introduction to perturbation techniques*. Wiley, New York, 1 edition, 1981.
- [23] J.P. Noel and G. Kerschen. Frequency-domain subspace identification for nonlinear mechanical systems. *Mechanical Systems and Signal Processing*, 40:701–717, 2013.
- [24] J.P. Noel and G. Kerschen. Nonlinear system identification in structural dynamics: 10 more years of progress. *Mechanical Systems and Signal Processing*, 83:2 – 35, 2017.
- [25] J.P. Noel, L. Renson, C. Grappasonni, and G. Kerschen. Identification of nonlinear normal modes of engineering structures under broadband forcing. *Mechanical Systems and Signal Processing*, 74:95–110.
- [26] J.P. Noel, S. Marchesiello, and G. Kerschen. Subspace-based identification of a nonlinear spacecraft in the time and frequency domains. *Mechanical Systems and Signal Processing*, 43:217–236, 2014.
- [27] L. Renson, A. D. Shaw, D. A.W. Barton, and S. A. Neild. Application of control-based continuation to a nonlinear structure with harmonically coupled modes. *Mechanical Systems and Signal Processing*, 120:449–464, apr 2019. ISSN 10961216. doi: 10.1016/j.ymssp.2018.10.008.

- [28] F. Schilder, E. Bureau, I.F. Santos, J.J. Thomsen, and J. Starke. Experimental bifurcation analysis continuation for noise-contaminated zero problems. *Journal of Sound and Vibration*, 358:251 – 266, 2015. ISSN 0022-460X. doi: <https://doi.org/10.1016/j.jsv.2015.08.008>.
- [29] R. Seydel. *Practical Bifurcation and Stability analysis*. Springer-Verlag, New York, 2010.
- [30] S.W. Shaw and C. Pierre. Normal modes for non-linear vibratory systems. *Journal of Sound and Vibration*, 164:85–124, 1993.
- [31] J. Sieber, A. Gonzalez-Buelga, S.A. Neild, D.J. Wagg, and B. Krauskopf. Experimental continuation of periodic orbits through a fold. *Physical Review Letters*, 100(24), jun 2008. ISSN 00319007. doi: 10.1103/PhysRevLett.100.244101.
- [32] B. Tang, M.J. Brennan, V. Lopes, S. Da Silva, and R. Ramlan. Using nonlinear jumps to estimate cubic stiffness nonlinearity: An experimental study. *Proceedings of the Institution of Mechanical Engineers, Part C: Journal of Mechanical Engineering Science*, 230(19):3575–3581, dec 2016. ISSN 20412983. doi: 10.1177/0954406215606746.
- [33] A.F. Vakakis. Non-linear normal modes and their applications in vibration theory: an overview. *Mechanical Systems and Signal Processing*, 11:3–22, 1997.

Appendix A. Analytical approximation of the response of the seventh-order forced Duffing-oscillator

To characterise our experimental rig, as a model we use a seventh-order, Duffing-like oscillator with the equation of motion given by (8):

$$\ddot{x} + b\dot{x} + \omega_n^2 x + \mu x^3 + \nu x^5 + \rho x^7 = \delta_{st}\omega_n^2 \cos(\omega t), \quad (A.1)$$

with a linear natural angular frequency ω_n , a static deflection δ_{st} , for the viscous damping b , and nonlinear coefficients μ , ν and ρ .

For the steady-state response of this system, one can derive an analytical approximate solution using the method of multiple scales [22]. Accordingly, we assume that a steady-state solution of (A.1) can be expanded in the following form

$$u(t) = u_0(t) + \varepsilon u_1(t) + \varepsilon^2 u_2(t) + \dots, \quad (A.2)$$

where u_0 is the fundamental harmonic component of the solution, considered as a steady-state solution of the linear, undamped, homogeneous system

$$\ddot{x} + \omega^2 x = 0, \quad (\text{A.3})$$

with a natural frequency equal to the forcing frequency, while ε is the perturbation parameter, which is assumed to be sufficiently small.

To simplify our formulae, we introduce dimensionless time as $\tau := \omega_n t$. Using the transformation $d/dt = \omega_n d/d\tau$ between the derivatives, the equation of motion (8) can be expressed as

$$x'' + \frac{b}{\omega_n} x' + x + \frac{\mu}{\omega_n^2} x^3 + \frac{\nu}{\omega_n^2} x^5 + \frac{\rho}{\omega_n^2} x^7 = \delta_{\text{st}} \cos(\omega t), \quad (\text{A.4})$$

where primes denote the derivation with respect to the dimensionless time τ . With the aim to express this equation with the homogenous system (A.3) and a nonlinear perturbation we introduce new coefficients for the nonlinear, damping and forcing terms $\hat{\mu} := \mu/(\varepsilon\omega_n^2)$, $\hat{\nu} := \nu/(\varepsilon\omega_n^2)$, $\hat{\rho} := \rho/(\varepsilon\omega_n^2)$, $\hat{b} := b/(\varepsilon\omega_n)$, as well as the frequency ratio $\zeta = \omega/\omega_n$. This yields to

$$x'' + x = \varepsilon \left(\frac{\delta_{\text{st}}}{\varepsilon} \cos(\zeta\tau) - \hat{b}x' - \hat{\mu}x^3 - \hat{\nu}x^5 - \hat{\rho}x^7 \right). \quad (\text{A.5})$$

Adding $\zeta^2 x$ to both sides, this equation can be re-arranged as

$$\omega_n^2 x'' + \zeta^2 x = \varepsilon \left(\frac{\zeta^2 - 1}{\varepsilon} x - \hat{b}x' - \hat{\mu}x^3 - \hat{\nu}x^5 - \hat{\rho}x^7 - \frac{\delta_{\text{st}}}{\varepsilon} \cos(\zeta\tau) \right). \quad (\text{A.6})$$

Introducing the parameters $\Psi := (\zeta^2 - 1)/\varepsilon$ and $\Phi := \hat{\delta}_{\text{st}}/\varepsilon$ we can express the equation of motion in the perturbed form of

$$\omega_n^2 x'' + \zeta^2 x = \varepsilon \left(\Psi x - \hat{b}x' - \hat{\mu}x^3 - \hat{\nu}x^5 - \hat{\rho}x^7 - \Phi \cos(\zeta\tau) \right). \quad (\text{A.7})$$

Substituting in the solution (A.2) and expanding equation (A.7) in a power series form by means of the perturbation parameter ε one obtains

$$u_0'' + \zeta^2 u_0 = 0, \quad (\text{A.8a})$$

$$u_1'' + \zeta^2 u_1 = \Psi u_0 - \hat{b}u_0' - \hat{\mu}u_0^3 - \hat{\nu}u_0^5 - \hat{\rho}u_0^7 + \Phi \cos(\zeta\tau), \quad (\text{A.8b})$$

$$u_2'' + \zeta^2 u_2 = \dots \quad (\text{A.8c})$$

The general solution of the homogenous ODE (A.8a) can be given as

$$u_0(\tau) = X \cos(\zeta\tau + \vartheta), \quad (\text{A.9})$$

with the vibration amplitude X and phase angle ϑ .

Note that this solution also contributes to the ‘forcing’ in the right-hand side of Eq. (A.8b). Moreover, u is a steady-state solution of (A.1) which implies that the functions $u_k, k = 1, 2, 3, \dots$ should be bounded: $|u_k(\tau)| \leq M$ for $\tau \in [0, \infty)$, $M \in \mathbb{R}^+$. Thus, the amplitude X and the phase angle ϑ in (A.9) should ensure that a non-resonant forcing is provided in Eq. (A.8b).

Substituting the solution (A.9) in Eq. (A.8b) yields to

$$\begin{aligned} u_1'' + \zeta^2 u_1 &= \Psi X \cos(\zeta\tau + \vartheta) + \zeta \hat{b} X \sin(\zeta\tau + \vartheta) \\ &\quad - \hat{\mu} X^3 \cos^3(\zeta\tau + \vartheta) - \hat{\nu} X^5 \cos^5(\zeta\tau + \vartheta) \\ &\quad - \hat{\rho} X^7 \cos^7(\zeta\tau + \vartheta) + \Phi \cos(\zeta\tau). \end{aligned} \quad (\text{A.10})$$

The linearization of the trigonometric expressions in the equation above provides

$$\begin{aligned} u_1'' + \zeta^2 u_1 &= \left(\frac{35}{64} X^7 \hat{\rho} + \frac{5}{8} X^5 \hat{\nu} + \frac{3}{4} X^3 \hat{\mu} - X \Psi - \Phi \cos(\vartheta) \right) \cos(\zeta\tau + \vartheta) \\ &\quad - \left(X \hat{b} \zeta + \Phi \sin(\vartheta) \right) \sin(\zeta\tau + \vartheta) + \dots, \end{aligned} \quad (\text{A.11})$$

where we include only the base harmonic terms, since these are the terms which could potentially trigger a resonance in Eq. (A.10). This can be avoided only if the coefficients of $\cos(\zeta\tau + \vartheta)$ and $\sin(\zeta\tau + \vartheta)$ are zero. That is

$$\frac{35}{64} X^7 \hat{\rho} + \frac{5}{8} X^5 \hat{\nu} + \frac{3}{4} X^3 \hat{\mu} - X \Psi - \Phi \cos(\vartheta) = 0, \quad (\text{A.12})$$

$$X \hat{b} \zeta + \Phi \sin(\vartheta) = 0. \quad (\text{A.13})$$

Using equations (A.12) and (A.13) one can derive an expression for the phase angle and the forcing amplitude each

$$\vartheta = \arctan \left(\frac{\hat{b} \zeta}{\Psi - \frac{35}{64} X^6 \hat{\rho} - \frac{5}{8} X^4 \hat{\nu} - \frac{3}{4} X^2 \hat{\mu}} \right), \quad (\text{A.14})$$

$$\Phi = \left| \frac{\frac{35}{64} X^7 \hat{\rho} + \frac{5}{8} X^5 \hat{\nu} + \frac{3}{4} X^3 \hat{\mu} - X \Psi}{\cos(\vartheta)} \right|. \quad (\text{A.15})$$

For the static deflection δ_{st} these provide

$$\vartheta = \arctan \left(\frac{\tilde{b}\zeta}{(\zeta^2 - 1) - \frac{35}{64}X^6\tilde{\rho} - \frac{5}{8}X^4\tilde{\nu} - \frac{3}{4}X^2\tilde{\mu}} \right), \quad (\text{A.16})$$

$$\delta_{\text{st}} = \left| \frac{\frac{35}{64}X^7\tilde{\rho} + \frac{5}{8}X^5\tilde{\nu} + \frac{3}{4}X^3\tilde{\mu} - X(\zeta^2 - 1)}{\cos(\vartheta)} \right|, \quad (\text{A.17})$$

with $\tilde{b} := \varepsilon\hat{b}$, $\tilde{\mu} := \varepsilon\hat{\mu}$, $\tilde{\nu} := \varepsilon\hat{\nu}$, $\tilde{\rho} := \varepsilon\hat{\rho}$.